Traffic 2010; **11:** 332–347

doi:10.1111/j.1600-0854.2009.01025.x

Mechanisms of Function of Tapasin, a Critical Major Histocompatibility Complex Class I Assembly Factor

Syed Monem Rizvi and Malini Raghavan*

Department of Microbiology and Immunology, University of Michigan Medical School, 5641 Medical Science Building II, Ann Arbor, MI 48109-5620, USA
**Corresponding author: Malini Raghavan, malinir@umich.edu*

For their efficient assembly in the endoplasmic reticulum (ER), major histocompatibility complex (MHC) class I molecules require the specific assembly factors transporter associated with antigen processing (TAP) and tapasin, as well as generic ER folding factors, including the oxidoreductases ERp57 and protein disulfide isomerase (PDI), and the chaperone calreticulin. TAP transports peptides from the cytosol into the ER. Tapasin promotes the assembly of MHC class I molecules with peptides. The formation of disulfide-linked conjugates of tapasin with ERp57 is suggested to be crucial for tapasin function. Important functional roles are also suggested for the tapasin transmembrane and cytoplasmic domains, sites of tapasin interaction with TAP. We show that interactions of tapasin with both TAP and ERp57 are correlated with strong MHC class I recruitment and assembly enhancement. The presence of the transmembrane/cytosolic regions of tapasin is critical for efficient tapasin–MHC class I binding in interferon-γ-treated cells, and contributes to an ERp57-independent mode of MHC class I assembly enhancement. A second ERp57-dependent mode of tapasin function correlates with enhanced MHC class I binding to tapasin and calreticulin. We also show that PDI binds to TAP in a tapasin-independent manner, but forms disulfide-linked conjugates with soluble tapasin. Thus, full-length tapasin is important for enhancing recruitment of MHC class I molecules and increasing specificity of tapasin–ERp57 conjugation. Furthermore, tapasin or the TAP/tapasin complex has an intrinsic ability to recruit MHC class I molecules and promote assembly, but also uses generic folding factors to enhance MHC class I recruitment and assembly.

Key words: Major histocompatibility complex class I, Tapasin, ERp57, Protein disulfide isomerase (PDI), calreticulin, TAP transporter

Received 17 July 2009, revised and accepted for publication 1 December 2009 uncorrected manuscript published online 3 December 2009, published online 8 January 2010

Major histocompatibility complex (MHC) class I molecules are activating ligands for T-cell receptors of $CD8^+$ T-cells, and the down-modulation of MHC class I molecules triggers immune recognition by natural killer cells. Thus, understanding the mechanisms of MHC class I assembly and cell surface expression is fundamental to many immune recognition processes. MHC class I molecules comprise a heavy chain, a light chain and a short peptide. Assembly of these components occurs in the endoplasmic reticulum (ER) of cells, and involves specific assembly factors for transporter associated with antigen processing (TAP) and tapasin, and generic ER chaperones. TAP is a critical factor comprising two subunits, TAP1 (ABCB2) and TAP2 (ABCB3), that are required for translocation of peptides from the cytosol into the ER (reviewed in 1). Tapasin is another critical cofactor required for the assembly of MHC class I heavy and light chain heterodimers with peptides (2,3).

Tapasin binds to TAP and increases steady-state levels of TAP, thereby allowing more peptides to be translocated into the ER (4,5). Truncated tapasin lacking the transmembrane and cytosolic regions (soluble tapasin) does not bind to TAP, but is able to bind MHC class I molecules and induces MHC class I cell surface expression to some extent (4). A disulfide-linkage is formed between the luminal cysteine 95 of tapasin and cysteine 57 of ERp57 (6,7). Tapasin–ERp57 binding was shown to enhance tapasin–MHC class I interactions as well as the functional activity of tapasin in reconstituted lysates and in tapasin-deficient cells (8,9). These studies have led to prevailing models that the transmembrane and cytosolic domains of tapasin are important for TAP stabilization and function, and that the ER luminal domains of tapasin are important for MHC class I recruitment and assembly enhancement. The tapasin–ERp57 conjugate is suggested to be the functional unit for recruiting MHC class I molecules and facilitating their peptide binding (8). However, purified soluble tapasin alone is able to interact with purified soluble MHC class I in a peptide-regulatable manner, but unable to induce MHC class I assembly with peptides (10). Purified soluble tapasin alone when tethered to purified MHC class I molecules via a Fos-Jun linkage is able to impact the assembly of MHC class I molecules with peptides (11). Furthermore, recent studies also suggest a role for the transmembrane/cytosolic region of tapasin for tapasin–MHC class I binding and for the functional activity of tapasin (12).

These different findings make it important to further understand the mechanisms of MHC class I recruitment to tapasin and of tapasin-mediated enhancement in the assembly of MHC class I molecules. Toward this end, we generated tapasin mutants lacking the ERp57 binding site [tapasin(C95A)], the TAP binding site (soluble tapasin), or both [soluble tapasin(C95A)]. Functional and interactions studies with these tapasin mutants provided important insights into the distinct modes of tapasin functions.

ERp57 is structurally and functionally related to PDI which was recently found to be associated with the TAP complex, and also suggested to be important for maintaining oxidized forms of TAP-associated MHC class I heavy chains (13). Some recent studies have questioned whether PDI is in fact recruited into the TAP complex (14 and references cited therein), and previous studies indicated that PDI did not form a disulfide-linked tapasin conjugate, under conditions where tapasin–ERp57 conjugates were observable (15). We also undertook analyses of interactions of PDI with TAP and tapasin in the context of the different tapasin mutants. These studies revealed a tapasin-independent mode of PDI–TAP association, and unexpected insights into the role of TAP–tapasin binding for enhancing specificity of tapasin–ERp57 conjugation.

Results

Reduced functional activities of soluble tapasin and tapasin(C95A) mutants

M553 is a tapasin-deficient human melanoma cell line with HLA-A2-haplotype loss (16). We examined the effects of the tapasin(C95A) mutation upon the abilities of full-length and soluble FLAG-tagged tapasin to induce cell surface expression of endogenous MHC class I of M553 cells (Figure 1A) and exogenously expressed influenza hemagglutinin-tagged HLA-A2 (M553/A2) (Figure 1B). Tapasin, when expressed exogenously, up-regulated MHC class I cell surface expression in M553 and M555/A2 cells (Figure 1A,B), as previously described (16). Tapasin also promoted assembly and ER exit of endogenously and exogenously expressed MHC class I molecules in M553 cells (data not shown). The soluble tapasin truncation reduced tapasin's ability to induce MHC class I surface expression, consistent with previous findings that TAP association is required for full function of tapasin (17,18) (Figure 1A,B). In the context of full-length tapasin, the C95A mutation also partially impacted tapasin's ability to induce endogenous MHC class I surface expression (Figure 1A) or exogenous influenza hemagglutinin-tagged HLA-A2 (A2) surface expression (Figure 1B), whereas in the context of soluble tapasin the C95A mutant had very low activity (Figure 1A,B). In M553 cells expressing wild-type soluble and full-length tapasin, class I expression (total steady-state class I) was enhanced compared with M553 alone (lacking tapasin) suggesting that wild-type soluble and full-length tapasin expression stabilized endogenous MHC class I in M553 cells (Figure 1A, lower panel, class I blot). Similar tapasin-mediated stabilization of exogenous class I (A2) was also observed (Figure 1B,

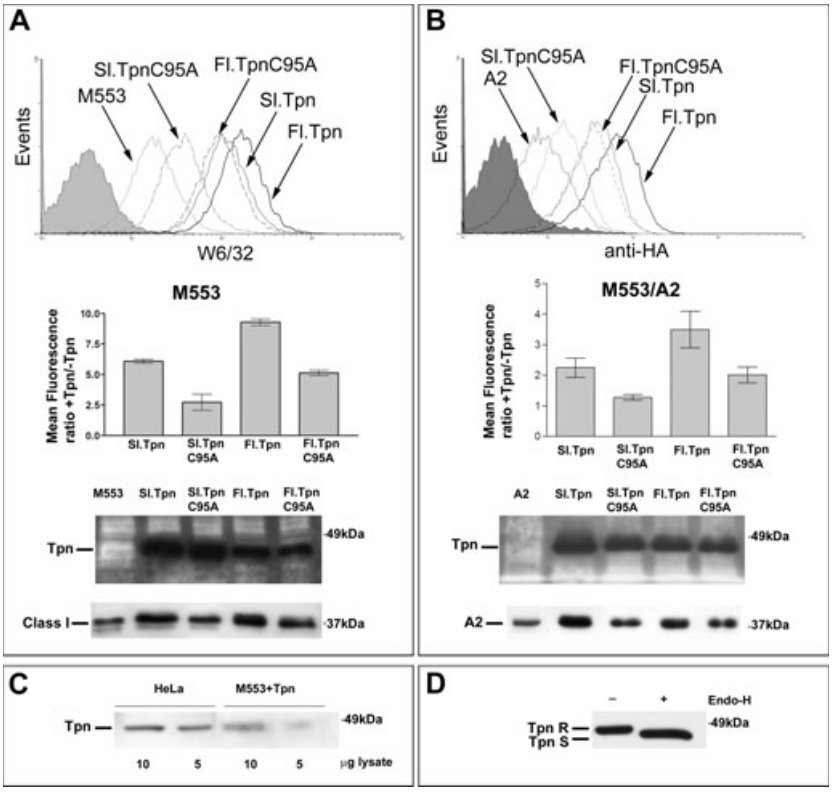

Figure 1: Tapasin truncations and C95A mutations affect surface expression and steady-state levels of endogenous and exogenous MHC class I molecules. A and B) Upper panels: Histogram showing cell surface expression of MHC class I in M553 or M553/A2 cells in the presence of the indicated tapasin constructs. Middle panels: Bar graphs shows mean fluorescence ratios of MHC class I expression as assessed by the W6/32 antibody (A) or anti-HA antibody (B) in the presence or absence of the indicated tapasin constructs. FACS data show average and standard error of mean of two independent analyses for (A) and four independent analyses for (B). Lower panel: Immunoblotting analysis using antibodies against tapasin and MHC class I [HC10 for (A) and anti-HA for (B)] of lysates from cells expressing the indicated proteins. C) Immunoblotting analysis using antibody against tapasin of lysates from HeLa cells and M553 cells expressing full-length tapasin. D) Immunoblotting analysis of lysates from M553 cells expressing soluble tapasin following no treatment or Endo-H digestion. Soluble tapasin and full-length tapasin are abbreviated as Sl.Tpn and Fl.Tpn, respectively. A total of 2×10^6 M553 or M553/A2 cells expressing indicated tapasin constructs were used per sample in the FACS analysis.Filled histogram shows control without primary antibody.

lower panel, A2 blot). Tapasin expression in M553 cells was comparable to the endogenous levels observed in other cell types such as HeLa cells (Figure 1C). The presence of the FLAG tag increased the molecular weight of soluble tapasin causing it to migrate very close to full-length tapasin when analyzed following SDS–PAGE and immunoblotting (Figure 1A,B, lower panel, tapasin blot). Under steady-state conditions, soluble tapasin remains completely Endo-H sensitive, indicating that it is retained in the ER of M553 cells (Figure 1D).

Tapasin mutations differentially impact binding to ERp57, MHC class I and calreticulin

Tapasin–ERp57 interaction was suggested to be critical for tapasin–MHC class I binding in some studies (8,9), whereas other studies have suggested a critical role for the transmembrane and cytosolic domains of tapasin in MHC class I binding (12). To further examine these possibilities, we undertook various co-immunoprecipitation studies. Efficient observation of tapasin binding to ERp57 and MHC class I in M553 cells required the use of a cross-linker such as dimethyl 3,3′ dithiobispropionimidate 2HCl (DTBP) or a thiol-modifying agent such as methyl methanethiosulfonate (MMTS). Using DTBP, a cell permeable cross-linker that was quenched prior to cell lysis, tapasin–ERp57 interactions were observed, and were C95-dependent in the context of both full-length and soluble tapasin as expected (Figure 2A,D). We believe this is evidence that specific C95-dependent interactions occur in cells and are not an artifact of interactions induced during cell lysis in MMTS. In all our binding studies, interferon-γ (IFN-γ) treatment of cells was also used to up-regulate TAP and enhance interactions that were potentially TAP-dependent, and also induce MHC class I expression for the interaction studies. Under these conditions, both full-length tapasin–MHC class I complexes were detectable with significantly higher efficiency than either soluble tapasin–MHC class I complex, and the C95A mutation reduced binding to MHC class I in the context of both full-length and soluble tapasin (Figure 2B,E). The tapasin–MHC class I binding was observable even in the context of soluble tapasin(C95A), consistent with our

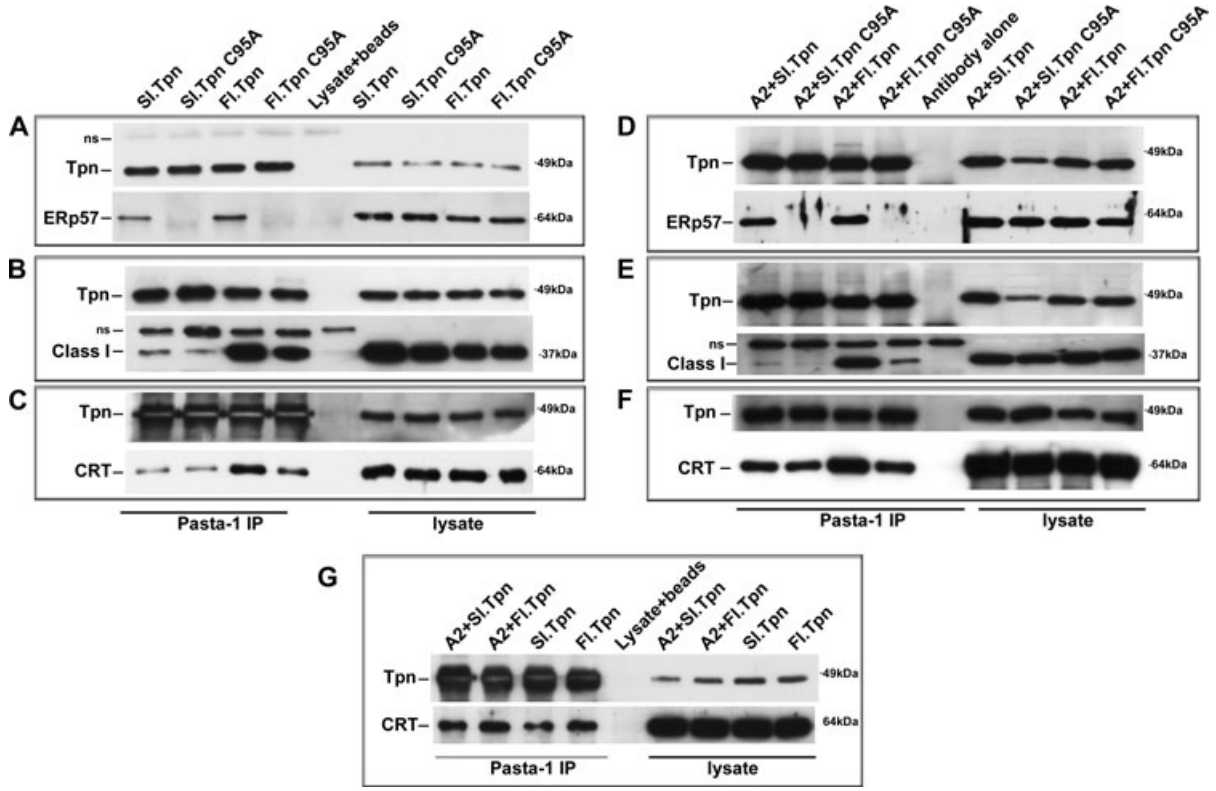

Figure 2: Tapasin truncations and C95A mutations impact tapasin–ERp57, tapasin–MHC class I and tapasin–calreticulin interactions. These analyses were conducted following cell treatments with IFN-γ for 48 h (A–G). 1.2–2.4 × 10^7 cells were treated with the membrane-permeable cross-linker DTBP immediately prior to lysis. Immunoblotting analysis with anti-tapasin (Pasta-1) immunoprecipitates or lysates from M553 (A–C), M553/A2 (D–F) or both (G) cells expressing indicated tapasin constructs. Antibodies specific for tapasin (Tpn), ERp57, calreticulin (CRT) and MHC class I were used in the immunoblotting analyses. Data are representative of two (A–G) or four (E) independent analyses. The lanes labeled lysate + beads correspond to the background bands obtained when lysates were immunoprecipitated with protein G beads (no antibody was used) and the lanes labeled antibody alone correspond to the background bands obtained when antibody was immunoprecipitated with buffer (no cell lysates were used). Ns, indicates non-specific bands that run above the tapasin or MHC class I heavy chain bands in the anti-tapasin and anti-class I blots.

previous finding that purified soluble tapasin and MHC class I are able to interact in the absence of all other components of the MHC class I assembly complex (10). However, this interaction is essentially functionally sterile in cells (Figure 1), as previously observed with the purified proteins (10).

Calreticulin is a component of MHC class I assembly complex (3), and calreticulin and ERp57 can interact independent of other MHC class I assembly components (19). In addition, tapasin- and ERp57-deficient cells have reduced abilities to recruit calreticulin into associations with the MHC class I assembly complex (20,21). Thus, investigations of the ERp57-dependence of tapasin–calreticulin binding were relevant. Calreticulin–tapasin binding was most efficiently detected in the context of full-length wild-type tapasin, and the C95A mutation reduced binding efficiency but did not abrogate binding, indicating that calreticulin association with tapasin was linked to ERp57 (Figure 2C,F), particularly in the context of full-length tapasin. Similar levels of calreticulin–tapasin interactions were observed when M553 and M553/A2 cells were compared within the same experiment, indicating that over-expression of MHC class I did not significantly impact the efficiency of calreticulin–tapasin binding under the conditions of the analyses (Figure 2G).

Compositions of TAP complexes are differentially impacted by tapasin mutations

On the basis of the previous studies (4,9), the transmembrane and cytosolic domains of tapasin are expected to be essential for TAP binding, and C95 of tapasin is expected to be essential for TAP–ERp57 binding and important for TAP–MHC class I and TAP–calreticulin binding. To further examine these requirements for tapasin in bridging different interactions to TAP in IFN-γ-treated cells, we undertook co-immunoprecipitation analyses with a TAP-specific antibody. TAP–tapasin binding was indeed strictly dependent on the presence of full-length tapasin (Figure 3A,E). No binding was observed between soluble tapasin and TAP1 in the anti-TAP1 immunoprecipitations (IPs) (Figure 3A,E), demonstrating the specificities of the interaction analyses in these assays. ERp57 binding to TAP1 was also tapasin-dependent, and required

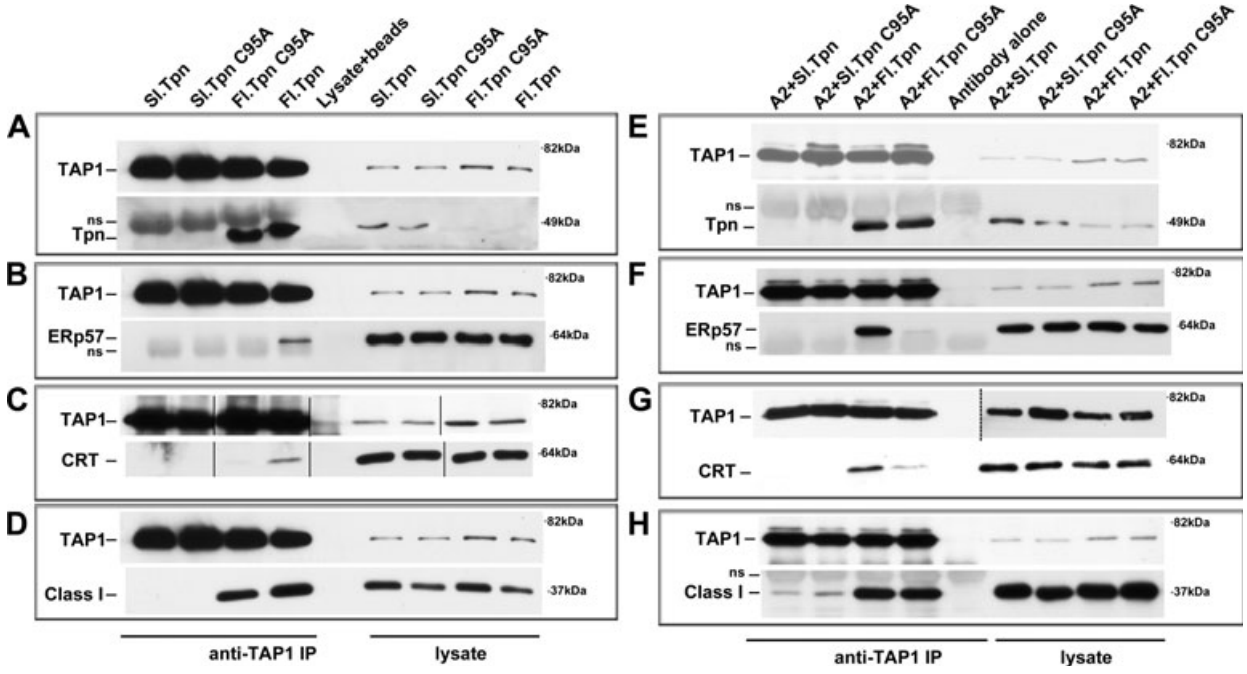

Figure 3: Tapasin truncations and C95A mutations impact the compositions of TAP complexes. The indicated cells were treated with IFN-γ for 48 h. For the analyses shown in panels E–H, 1.2–2.4 × 10^7 cells were treated with the membrane-permeable cross-linker DTBP immediately prior to lysis. The analyses in panels A–D did not use a cross-linker. A–H) Immunoblotting analysis of anti-TAP1 immunoprecipitates or lysates from M553 (A–D) or M553/A2 (E–H) cells expressing indicated tapasin constructs. Antibodies specific for TAP1, tapasin (Tpn), MHC class I heavy chain, ERp57 and calreticulin (CRT) were used. Data are representative of two (A–H) or four (F) independent analyses. The lanes labeled lysate + beads correspond to the background bands obtained when lysates were immunoprecipitated with protein G beads (in the absence of antibody) and the lanes labeled antibody alone correspond to the background bands obtained when antibody was immunoprecipitated with buffer (no cell lysates were used). Solid lines in panel C indicate lanes that were cut and pasted from the same blot in order to preserve the order of presentation of lanes. Dashed lines in panel G indicate different exposures shown for immunoprecipitates and lysates of TAP1 blots from within the same experiment. Ns indicates antibody-derived non-specific bands that run above the tapasin and class I bands in blots with anti-tapasin, anti-class I and below the ERp57 band in blots with anti-ERp57 (IP lanes only).

the presence of C95 of tapasin (Figure 3B,F). Furthermore, calreticulin binding to TAP was ERp57-linked (Figure 3C,G). Finally, MHC class I association with TAP was also strongly tapasin-dependent, but at best only partly impacted by the C95A mutation (Figure 3D,H), consistent with the findings of Figure 2. TAP1 interactions with indicated proteins were stable, and interactions were detectable both in the absence (Figure 3A–D) and in the presence of cross-linker (Figure 3E–H). Together, these findings indicate that ERp57 association with TAP is dependent on tapasin and requires an intact tapasin C95, that calreticulin association with TAP is ERp57-linked, and that MHC class I association with TAP is strongly tapasin-dependent, but only partly linked to C95 of tapasin.

MHC class I-calreticulin binding is significantly impacted by tapasin(C95A) mutations

The binding studies of Figure 2 undertaken with an anti-tapasin antibody revealed that soluble tapasin truncation impaired tapasin–MHC class I binding more significantly than the tapasin(C95A) mutation, indicating that the tapasin transmembrane/cytosolic regions indirectly or directly stabilized tapasin–MHC class I binding. Similar results were obtained when the immunoprecipitation analyses were undertaken with an anti-MHC class I (HC-10) antibody (Figure 4A,B). HC-10 was used as it has previously been shown to efficiently detect tapasin–MHC class I complexes (22). ERp57 binding to MHC class I was readily detectable in the context of full-length tapasin (Figure 4A,B), and weakly detectable in the context of soluble tapasin (Figure 4B) likely reflecting the indirect tapasin-mediated association between ERp57 and MHC class I heavy chains. Despite weaker MHC class I binding by soluble tapasin compared with the full-length tapasin(C95A) mutant, soluble tapasin was able to induce MHC class I to a level similar to or greater than that induced by full-length tapasin(C95A), both in the absence of IFN-γ (Figure 1) and in the presence of IFN-γ (Figure 4C). Functional activity of soluble tapasin correlated with its ability to more efficiently recruit calreticulin into association with MHC class I molecules, compared with tapasin(C95A) (Figure 4A,B). Calreticulin binding to MHC class I was detected most efficiently in the presence of full-length tapasin, and additionally, calreticulin binding was enhanced in the context of wild-type and soluble tapasin compared with either C95A mutant (Figure 4A,B). Together, these results suggest that the ability to recruit calreticulin into associations with MHC class I molecules in an ERp57-dependent manner may underlie the observed functional activity of soluble tapasin. ERp57 association with tapasin brings calreticulin into proximity with MHC class I, which may be related to the enhancements in steady-state MHC class I in cell lysates in the context of full-length or soluble tapasin (Figure 1A,B, lower panels).

Tapasin(C95A) facilitates assembly of MHC class I independent of its functions in TAP stabilization

Pulse chase and Endo-H digestion analyses showed that, in cells lacking tapasin, MHC class I molecules were retained in the ER and did not mature even after 120 min. In contrast, in the presence of full-length tapasin(C95A), maturation of MHC class I molecules was accelerated, indicating that tapasin(C95A) actively promoted assembly of MHC class I molecules and their ER exit (Figure 5A). Use of wild-type tapasin further enhanced maturation of MHC class I heavy chains (data not shown). The ability of full-length tapasin(C95A) to induce MHC class I assembly and cell surface expression (Figures 1 and 5A) could be related to tapasin(C95A)-mediated induction of TAP steady-state levels (4,5), an intrinsic assembly promoting function of tapasin(C95A), or tapasin(C95A)-dependent tethering of MHC class I molecules into a physical association with TAP. To further examine the first possibility, we compared the effects of IFN-γ treatment of M553 cells upon the cell surface expression of MHC class I in M553 cells and in M553 cells expressing full-length tapasin(C95A) (Figure 5B). IFN-γ up-regulated MHC class I cell surface expression in both cells with a more significant effect being observed in the presence of full-length tapasin(C95A) (Figure 5B). Comparison of steady-state levels of TAP and MHC class I in IFN-γ-treated cells or tapasin(C95A)-expressing cells revealed that under the conditions of the analyses, IFN-γ treatment had a much more profound effect on steady-state levels of TAP1 and MHC class I, compared with that induced by tapasin(C95A) expression (Figure 5C,D). In addition, higher levels of TAP1/TAP2 complexes were induced by IFN-γ-treatment, as assessed by immunoprecipitations with anti-TAP1, followed by immunoblotting analyses for TAP2 (Figure 5D).

Despite the stronger induction of active TAP complexes and MHC class I molecules in IFN-γ-treated M553 cells, cell surface MHC class I expression was consistently lower than that induced by tapasin(C95A), arguing that the mechanism of tapasin(C95A) function did not relate to its ability to stabilize TAP complexes *per se*. Rather, the functional activity of full-length tapasin(C95A) relates either to its intrinsic ability to bind MHC class I and promote peptide loading of MHC class I, or to its ability to induce a physical association between MHC class I and the TAP complex.

PDI associates with TAP in a tapasin-independent manner

PDI has previously been shown to be associate with TAP (13), but the tapasin dependence of this interaction is not well-characterized. We examined the interactions of PDI with TAP, in the context of the different tapasin mutations. In contrast to the ERp57–TAP1 interaction which was completely dependent on the presence of tapasin (Figure 3B,F), PDI interaction with TAP was readily detected in the presence of both soluble tapasin constructs, indicating a tapasin-independent TAP–PDI

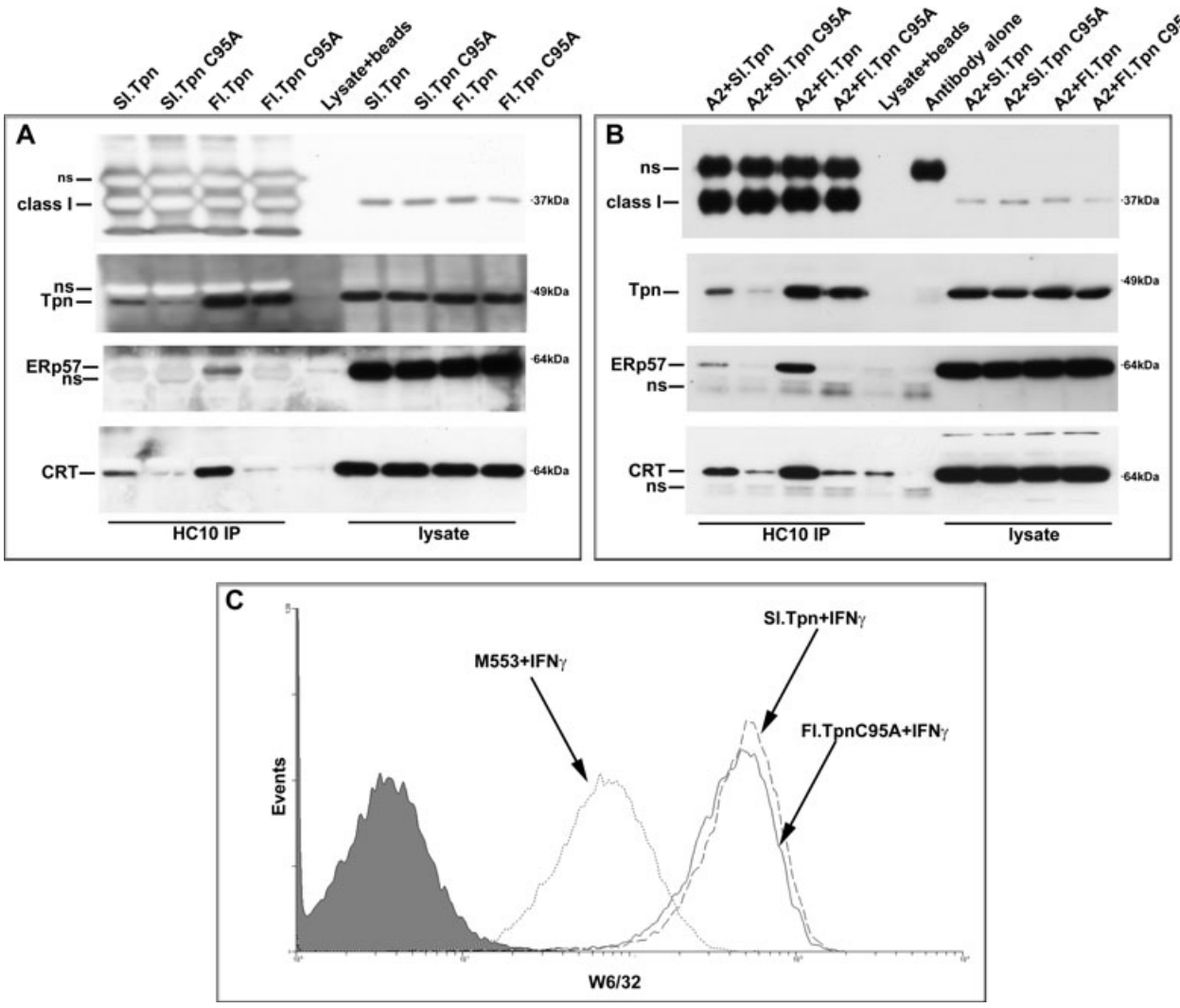

Figure 4: Tapasin truncations and C95A mutations impact MHC class I–tapasin and MHC class I–calreticulin interactions. These analyses were conducted following cell treatments with IFN-γ for 48 h. A total of 1.2–2.4 × 10^7 cells were treated with the membrane-permeable cross-linker DTBP immediately prior to lysis. Immunoblotting analysis with anti-MHC class I (HC10) of immunoprecipitates or lysates from M553 (A) or M553/A2 (B) cells expressing indicated tapasin constructs. Samples for all panels of (A) and (B) were derived from the same immunoprecipitation experiment, respectively, and thus a single MHC class I panel is shown for each. Antibodies specific for MHC class I, tapasin (Tpn), ERp57 and calreticulin (CRT) were used in the immunoblotting analyses. C) Histograms showing cell surface expression of MHC class I in M553 or M553 cells expressing soluble tapasin or full-length tapasin(C95A) following treatment with IFN-γ (500 IU) for 48 h (conditions similar to those under which binding studies were undertaken). Filled histogram shows control staining without primary antibody. Data are representative of one (C) or at least two independent analyses for each panel of (A) and (B). The lanes labeled lysate + beads correspond to the background bands obtained when lysates were immunoprecipitated with protein G beads (no antibody was used) and the lanes labeled antibody alone correspond to the background bands obtained when antibody was immunoprecipitated with buffer (no cell lysates were used). Ns, indicates non-specific bands.

interaction (Figure 6A,B). This result was confirmed in tapasin-deficient M553 cells (Figure 6C). In fact, the absence of tapasin in association with TAP appeared to enhance PDI–TAP associations (Figure 6A,C). TAP1–PDI interactions were also verified in other human cell types with an intact MHC class I assembly complex, such as HeLa cells (Figure 6D) and the TAP1-deficient SK-mel-19 cells that express TAP1 exogenously (data not shown).

The soluble tapasin truncation induces tapasin–PDI conjugation

Both PDI and ERp57 are associated with TAP (Figures 3 and 6), but tapasin conjugate formation is reported to be specifically induced with ERp57 (15). We re-examined whether PDI is able to form disulfide-linked conjugates with the tapasin constructs used in this study. For these analyses, IFN-γ-treated cells were lysed in the presence

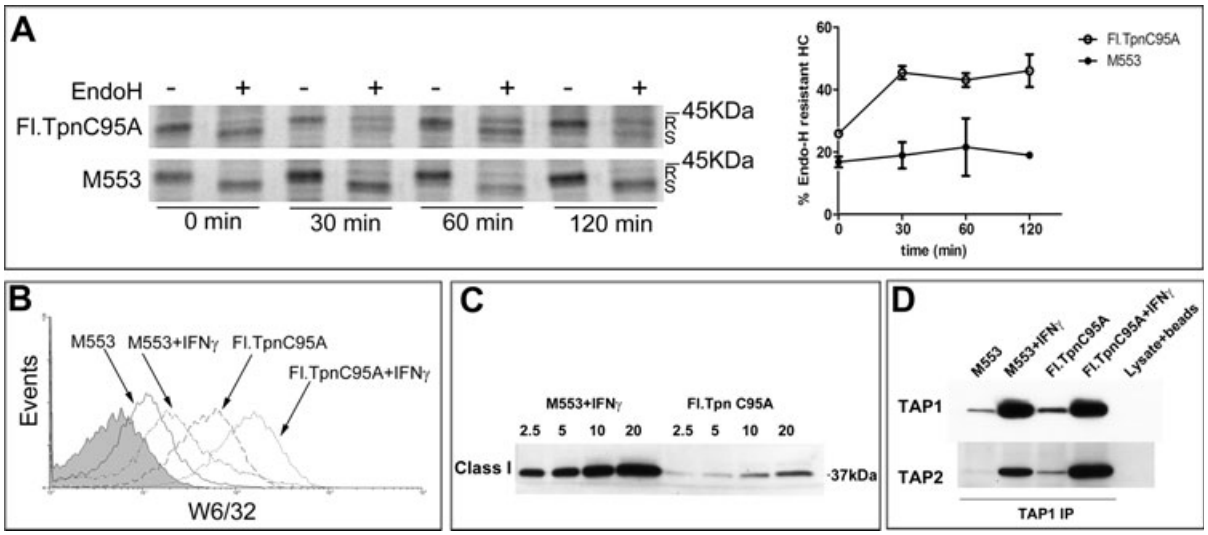

Figure 5: The tapasin(C95A) mutant induces MHC class I assembly independent of an effect on TAP stabilization. A) Left panel: M553 or full-length tapasin(C95A) expressing M553 cells were metabolically labeled for 10 min and chased for the indicated times in fresh media. Lysates were immunoprecipitated with W6/32, then digested with Endo-H or left undigested and analyzed by SDS–PAGE and phosphorimaging analyses. Right panel: The Endo-H resistant MHC class I heavy chain (HC) bands in above gels were quantified using IMAGEQUANT and plotted as a percentage of Endo-H resistant HC. Data are representative of two independent analyses. B) Histograms showing cell surface expression of MHC class I in M553 or M553 cells expressing full-length tapasin(C95A) following no treatment or following incubation with IFN-γ (500 IU) for 20 h. C) Immunoblotting analysis using HC10 of indicated amounts of total cell lysates from IFN-γ-treated M553 cells or tapasin(C95A)-expressing M553 cells. D) Immunoblotting analysis of anti-TAP1 immunoprecipitates of IFN-γ-treated or untreated M553 and tapasin(C95A)-expressing cells. Antibodies specific for TAP1 and TAP2 were used.

of MMTS (without cross-linker), and immunoblotting analyses of lysates or anti-tapasin immunoprecipitates were undertaken following SDS–PAGE under reducing or non-reducing conditions.

Although the major ERp57 conjugate observable in cell lysates corresponded to the size of the tapasin–ERp57 conjugate (Figure 7B, lanes 6 and 8), several PDI conjugates were observable (Figure 7C, lanes 6 and 8), suggesting that mixed disulfides between PDI and cellular proteins are more stable or more numerous than those with ERp57. That tapasin is a uniquely detectable cellular substrate of ERp57 has previously been documented, and the stable disulfide-linkage between tapasin and ERp57 is attributed to an additional non-covalent interaction between the proteins (15). In the absence of chemical cross-linkers (not used to derive the data of Figure 7) or trapping mutants of ERp57, mixed disulfide formation with ERp57 is previously only reported in the context of tapasin (15) or viral glycoproteins (23).

In immunoprecipitations with the tapasin-specific antibody (Pasta-1) (6), as expected, conjugates of 110 kDa were observed under non-reducing conditions with both full-length and soluble tapasin, and were detectable in immunoblotting analyses with anti-tapasin as well as anti-ERp57 (Figures 7A,B). These conjugates were C95-dependent (data not shown). In addition, a PDI conjugate of 110 kDa was observed in immunoprecipitates from cells expressing soluble tapasin (Figure 7C, lane 1). A much weaker signal for PDI was obtained under reducing conditions, indicating that the anti-PDI antibody preferentially detects the conjugated form of PDI (Figure 7C, lane 1 compared with lane 2) (this band is more readily detectable in longer exposures of the PDI blot; data not shown). The PDI conjugate of 110 kDa was undetectable or very weak in the context of full-length tapasin (Figure 7C, lane 1 compared with lane 3), consistent with the previous findings that full-length tapasin PDI conjugates are not readily detectable (15). The 110 kDa PDI conjugate in the context of soluble tapasin was not observed in Pasta-1 immunoprecipitates of cells expressing soluble or full-length tapasin(C95A) (data not shown).

To further characterize whether PDI did form conjugates with soluble tapasin, and to quantify the extent of conjugate formation, elution profiles of soluble tapasin and soluble tapasin(C95A) were compared following lysis of the corresponding M553 cells in MMTS (without cross-linker), anti-FLAG-based purifications of soluble tapasin and associated proteins, and further gel filtration-based separation of free tapasin or its conjugates. Relevant fractions were analyzed by reducing (Figure 8A, left panels) or non-reducing (Figure 8A, right panels) SDS–PAGE and immunoblotting analyses for tapasin, ERp57 and PDI. Soluble tapasin was indeed in conjugate with both ERp57 and PDI in fractions B2–C2, and fractions C3–C5 contained majority of free tapasin (Figure 8A). Bands corresponding to a tri-molecular complexes (Tapasin–ERp57–PDI) were not visualized

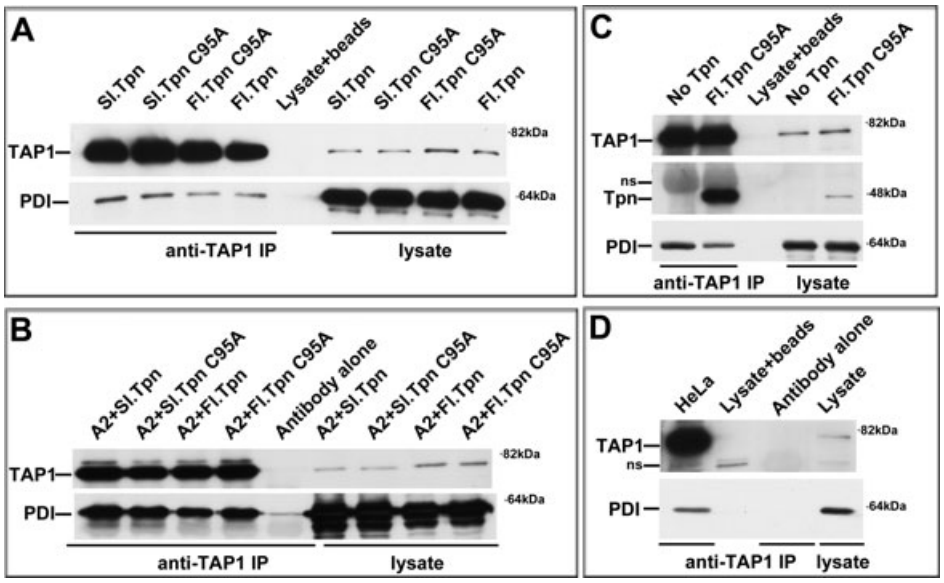

Figure 6: Tapasin-independent association of PDI with TAP. The indicated cells were treated with IFN-γ for 48 h. For panel (B), cells were treated with the membrane-permeable cross-linker DTBP immediately prior to lysis, and the analyses of panels (A), (C) and (D) were undertaken without cross-linker treatment. A and B) Immunoblotting analysis of anti-TAP1 immunoprecipitates or lysates from M553 (A) or M553/A2 cells (B) expressing indicated tapasin constructs. C) Immunoblotting analysis of anti-TAP1 immunoprecipitates or lysates from parent M553 cells lacking tapasin expression (No Tpn) or M553 cells expressing full-length tapasin(C95A) as indicated. D) Immunoblotting analysis of anti-TAP1 immunoprecipitates or lysates from HeLa cells. Antibodies specific for TAP1, PDI were used in the immunoblots. Data are representative of one (C) or two (A, B and D) independent analyses. The lanes labeled lysate + beads correspond to the background bands obtained when lysates were immunoprecipitated with protein G beads and the lanes labeled antibody alone correspond to the background bands obtained when antibody was immunoprecipitated with buffer (no cell lysates were used). Ns indicate non-specific antibody-derived band that runs above the tapasin band or a non-specific band that runs below the TAP1 band.

in the non-reducing gels (Figure 8A), suggesting that only heterodimers of soluble tapasin–ERp57 and soluble tapasin–PDI were present. Although weak signals for a few higher molecular weight band above 110 kDa were detected in the ERp57 blots (Figure 8A, fractions B1–C1), these bands were absent in the PDI blots suggesting that they do not represent a tri-molecular complex between tapasin–ERp57–PDI. The identity of these higher molecular weight bands in the ERp57 blot is unknown. Neither ERp57 nor PDI was visualized in eluates from cells expressing soluble tapasin(C95A) (data not shown), confirming that both conjugates with tapasin were C95-dependent. These findings suggest that PDI-soluble tapasin conjugates are unlikely to be folding intermediates, but rather represent a deviation from the specificity of tapasin conjugation to ERp57.

Soluble tapasin purified from lysates of M553 cells was mainly observed to migrate at the expected position for tapasin–ERp57 or tapasin–PDI conjugate (Figure 8A, fractions B2–C2) or tapasin monomer (Figure 8A, fractions C3–C5) and only a small amount was observed in the void volume of the column (Figure 8A, fractions B12–B11). Soluble tapasin(C95A) migrated at the expected position of monomer, and only a small fraction was present in the column void volume (data not shown). Thus, at the levels expressed in M553 cells, neither soluble tapasin nor soluble tapasin(C95A) derived from cell lysates appeared to be significantly aggregated.

The relative amounts of PDI and ERp57 that were associated with soluble tapasin were quantified by two different methods. Fractions containing conjugates were pooled following the gel filtration chromatography, concentrated, separated by SDS–PAGE and visualized by Coomassie staining (Figure 8B). Mass spectrometric analyses of band 1 yielded several proteins including ERp72 and GRp78. Mass spectrometric analysis of band 2 yielded ERp57 and PDI as the two most abundant proteins. The averaged intensity of the 10 most abundant ERp57 peptides was 3.2×10^7, 7.5-fold higher than the averaged intensity of the 10 most abundant PDI peptides (4.2×10^6) (Figure S1). This corresponds to PDI representation at a level of 13.3% relative to ERp57. Mass spectrometric quantifications of the relative abundance of ERp57 and PDI were verified by the titration of tapasin conjugates against known amounts of purified ERp57 and PDI in immunoblotting analyses (Figure 8C). Band intensities of the purified PDI and ERp57 standards were plotted as a function of protein concentration, linearly fitted, and the relative concentration of each protein in the conjugates calculated. These analyses suggested PDI representation at a level of 12% relative to ERp57. Together, these analyses indicate that although

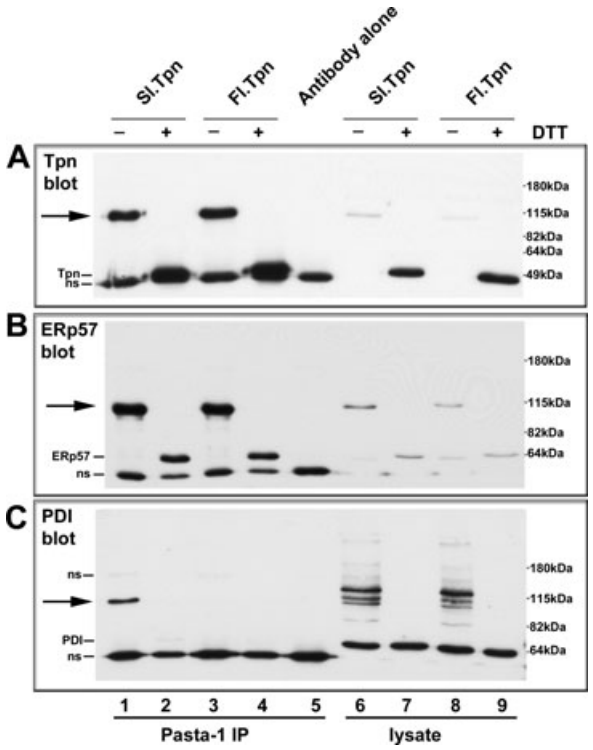

Figure 7: Soluble tapasin truncation induces tapasin–PDI conjugation. M553 cells expressing different tapasin constructs were treated with IFN-γ and lysed in the presence of MMTS (no cross-linker) and immunoprecipitated with Pasta-1 to study tapasin conjugates with ERp57 and PDI. A–C) Following lysis in the presence of MMTS, Pasta-1 immunoprecipitates or lysates from M553 cells expressing the indicated tapasin constructs were analyzed by immunoblotting, using antibodies specific for tapasin, ERp57 and PDI. Arrows indicate the migration positions of DTT-sensitive bands (conjugates) of approximately 110 kDa. Proteins were separated by reducing (+DTT) and non-reducing (−DTT) SDS–PAGE as indicated, prior to immunoblotting analyses. Non-specific antibody-derived bands that migrate below the tapasin, ERp57 and PDI bands in the corresponding blots are indicated by ns.

soluble tapasin is preferentially associated with ERp57, conjugation to PDI is observable at a level that is not insignificant.

Heterologous expression of soluble human tapasin induces associations with several endogenous oxidoreductases, and aggregation of secreted but not intracellular versions

We previously reported that purification of soluble tapasin from supernatants of CHO cells over-expressing soluble human tapasin and cultured at 37°C yielded protein that was largely aggregated (Figure 9A, dashed chromatogram). Aggregation could be suppressed by culturing the cells at 30°C (10). Surprisingly, soluble tapasin purified from lysates of the CHO cells cultured at 37°C and lysed in the presence of MMTS yielded two major peaks (Figure 9A, solid chromatogram), corresponding to tapasin–oxidoreductase conjugates (peak 2, Figure 9B) or free tapasin (peak 3, Figure 9B), rather than aggregated protein in the void volume (peak 1, Figure 9A). SDS–PAGE analyses of proteins present in peak 2 revealed the presence of several protein bands in addition to tapasin. Mass spectrometric analyses of bands from peak 2 indicated the presence of peptides corresponding to both ERp57 and PDI, as well as those corresponding to GRP78 and ERp72. The ERp57/PDI bands were partially displaced (Figure 9B, peak 2, lane 1 compared with lane 2) when the peak was analyzed following soluble tapasin purification from lysates of CHO cells co-expressing soluble tapasin and human ERp57 lacking an ER retention motif (Figure 9C,D). Regardless of human ERp57 co-expression, cell lysate-derived soluble tapasin was present as conjugates or free tapasin monomers, whereas the cell supernatant-derived soluble tapasin was largely aggregated (Figure 9A,D). In the absence of human ERp57 co-expression, soluble tapasin associated with endogenous hamster cell-derived oxidoreductases and chaperones, and some of the interactions persisted despite human ERp57 co-expression. Thus, ER–lumenal interactions were critical for inhibition of soluble tapasin aggregation, and soluble tapasin formed conjugates with several oxidoreductases in hamster cells.

ERp57 representation correlates with calreticulin recruitment to purified soluble tapasin conjugates

To further study the effect of ERp57 on calreticulin recruitment to tapasin, we isolated tapasin from lysates of CHO cells expressing human tapasin alone or human tapasin and ERp57 (Figure 9E). CHO cells expressing tapasin alone were lysed in the presence and in the absence of MMTS, whereas CHO cells expressing both human tapasin and human ERp57 were lysed in the presence of MMTS. The three sets of purified proteins were analyzed by immunoblotting analyses with antibodies directed against tapasin, ERp57 and PDI. ERp57 representation in eluates from the anti-FLAG column correlated with human ERp57 co-expression, as well as the presence of MMTS during cell lyses (Figure 9E, ERp57 blot, lanes 7–9 compared with lanes 1–6). Conversely, human ERp57 co-expression reduced PDI association with tapasin (Figure 9E, PDI blot, lanes 7–9 compared with lanes 4–6). In the absence of MMTS during lysis, recovery of both ERp57 and PDI were relatively inefficient or not observable (Figure 9E, ERp57 and PDI blots, lanes 1–3 compared with lanes 4–9). The purified protein preparations or BSA were immobilized in 96-well microtitration plates, and calreticulin binding to each protein or BSA was compared by enzyme-linked immunosorbent assay (ELISA) (Figure 9F). Calreticulin showed more binding to each tapasin preparation compared with the control protein BSA (Figure 9F). The preparation that had the highest level of ERp57 representation displayed the strongest binding to calreticulin (Figure 9F). Thus, in these *in vitro* binding assays as in cells, ERp57 binding to tapasin

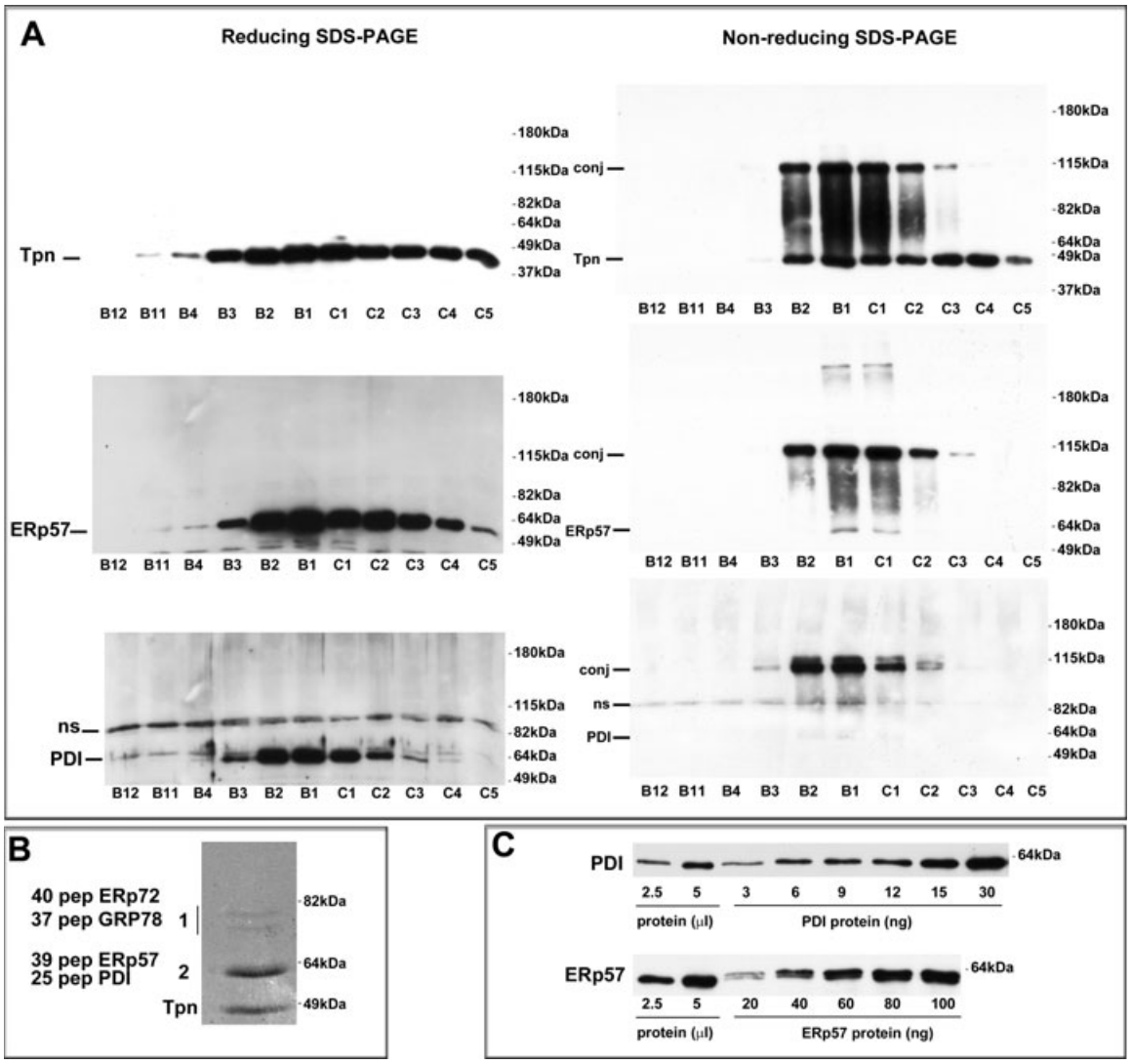

Figure 8: PDI forms C95-dependent conjugates with soluble tapasin at reduced levels compared with ERp57. A total of 4.8×10^7 M553/soluble tapasin cells were lysed in the presence of MMTS (no cross-linker) and immunoprecipitated with anti-FLAG beads to study tapasin interaction with ERp57 and PDI by gel filtration analysis. A) Gel filtration-based separation of proteins derived from M553/soluble tapasin following lysis in MMTS, and anti-FLAG-based affinity purification of soluble tapasin. Fractions were analyzed for the presence of tapasin (Tpn), PDI and ERp57 by immunoblotting analyses, following SDS–PAGE under reducing (left panels) or non-reducing conditions (right panels). B and C) Following gel filtration and pooling/concentration of fractions containing conjugates, proteins were resolved by SDS–PAGE, Coomassie stained, and indicated bands 1 and 2 were subjected to mass spectrometric analyses (B) or titrated against indicated concentrations of purified PDI (C, top panel) and ERp57 (C, Lower panel) in immunoblotting analyses. For (B), proteins identified by mass spectroscopic analyses in bands 1 and 2 and the number of peptides identified for each protein are indicated. For (C), band intensities were quantified by IMAGEQUANT and plotted as a function of PDI or ERp57 concentration. Linear regression analyses and interpolation from the standard curves allowed estimation of protein amounts in the conjugates. On the basis of these analyses, 5 μL conjugate is estimated to contain 75.3 ng ERp57 and 9.1 ng PDI.

enhances the recruitment of calreticulin. As per the data of Figure 4A,B, it appears that the ERp57-associated form of calreticulin must also be able to interact with tapasin-associated MHC class I. It is possible that this binding contributes to the observed enhancement in stability of the tapasin–MHC class complex (Figure 4A,B) in the context of tapasin–ERp57 complexes.

Discussion

The studies described here demonstrate that weak intrinsic interactions between the lumenal domains of tapasin and MHC class I are strongly enhanced by the presence of the transmembrane and cytosolic domains of tapasin, and also enhanced by tapasin–ERp57 binding

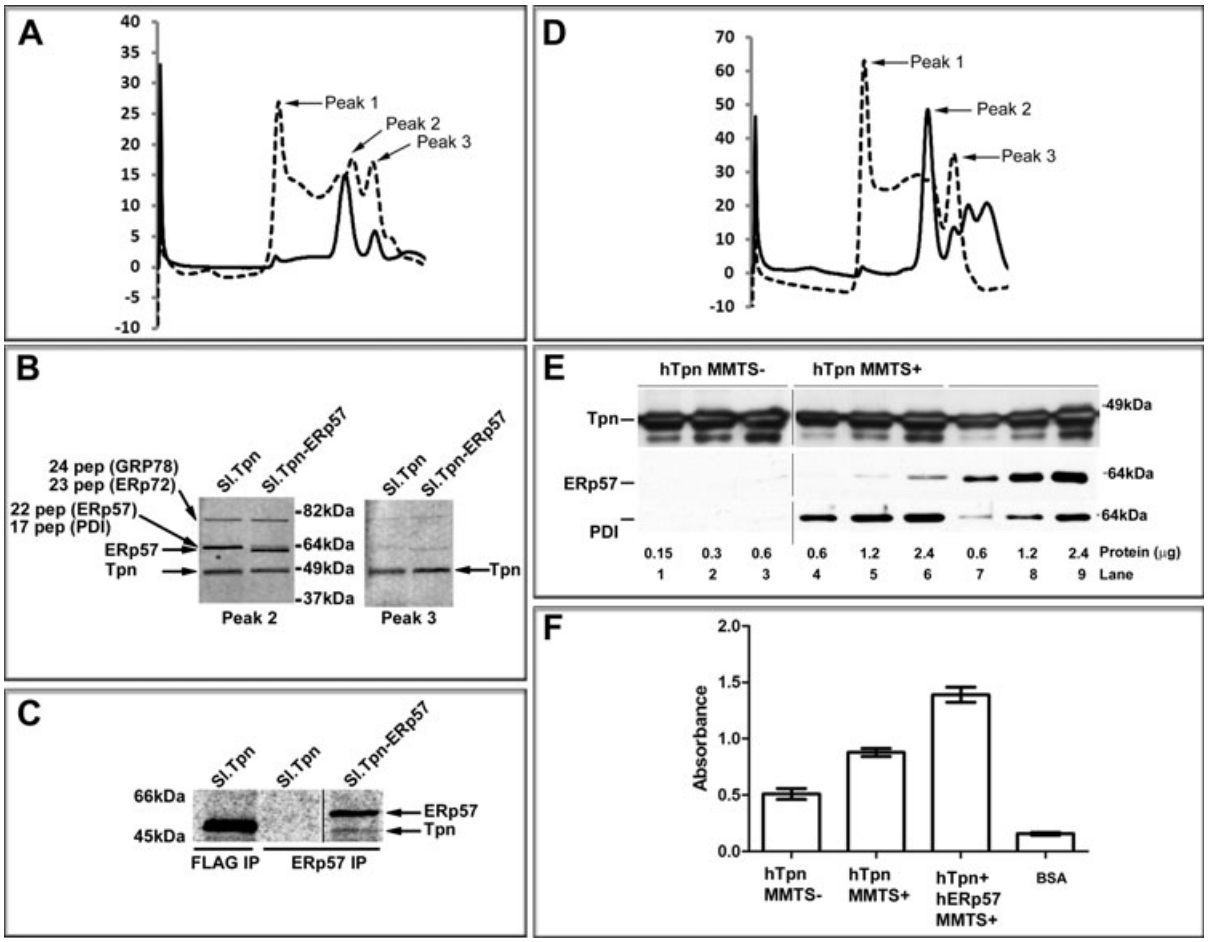

Figure 9: Purification of different tapasin conjugates from CHO cells and their use in calreticulin binding studies. A and D) Gel filtration chromatograms of soluble tapasin purified from supernatants (dotted lines) or lysates of MMTS-treated (solid lines) CHO cells expressing soluble tapasin alone (A) or soluble tapasin and ERp57 (D). Peaks corresponding to gel filtration column void volume (peak 1), tapasin-oxidoreductase conjugates (peak 2) and free tapasin (peak 3) are indicated by arrows. B) Fractions corresponding to the peaks 2 and 3 of the cell lysate-based chromatograms shown in (A) and (D) were analyzed by SDS–PAGE and Coomassie Blue staining. Arrows indicate proteins identified by mass spectroscopic analyses of the peak 2 fractions from CHO cells expressing soluble tapasin, and the number of peptides identified for each protein. C) Metabolic labeling, immunoprecipitation (with indicated antibodies), SDS–PAGE and phosphorimaging analyses of supernatants from CHO cells expressing soluble tapasin and ERp57 or soluble tapasin alone, to indicate that both tapasin and ERp57 or tapasin alone were expressed in the supernatants. Solid line in panel (C) indicates a lane that was cut and pasted from a different gel within the same experiment. E) Immunoblot analysis of purified tapasin proteins, with antibodies directed against tapasin, ERp57 and PDI as indicated. Lanes 1–3, tapasin purified from CHO–tapasin cells lysed in the absence of MMTS. Lanes 4–6, tapasin purified from CHO–tapasin cells lysed in the presence of MMTS. Lanes 7–9, tapasin purified from CHO–tapasin–human ERp57 cells lysed in the presence of MMTS. Solid lines indicate lanes that were cut and pasted from the same blots. F) 96-well ELISA plates were coated overnight with 1–2 μg of indicated tapasin proteins or BSA as control, and binding to purified calreticulin was analyzed by ELISA. All incubation and wash steps were undertaken in the presence of 0.5 mM $CaCl_2$. Absorbance values obtained from duplicate readings were used to plot the graph. The data is average of two independent analyses.

(Figures 2 and 4). The inability to recruit ERp57 strongly impairs the functional activity of soluble tapasin(C95A), which is a weak inducer of MHC class I assembly (Figure 1). Although the C95A mutation also reduces the functional activity of full-length tapasin, significant ERp57 binding-independent functional activity is measurable with full-length tapasin(C95A), which is not strongly correlated with tapasin-mediated stabilization of TAP (Figures 1 and 5). The tapasin(C95A) mutation also impacts the efficiency of calreticulin recruitment to MHC class I molecules (Figure 4). Although ERp57 and calreticulin binding to TAP are strongly dependent on or linked to tapasin(C95), PDI association with TAP is tapasin-independent, and in fact association appears to be enhanced by the absence of tapasin or a fully functional tapasin molecule. These findings indicate distinct modes of binding and distinct functions for ERp57 and PDI within MHC class I assembly complexes. Significant C95-dependent conjugation of PDI

to tapasin is only detectable in the context of soluble tapasin, studies that point to the importance of full-length tapasin for enhancing specificity of interactions within MHC class I assembly complexes.

The panel of mutants described here was also characterized in a recent report from the Cresswell laboratory (24), published while this manuscript was under revision. Although the two studies come to similar conclusions about the importance of both tapasin–ERp57 binding and the transmembrane/cytosolic regions of tapasin in its interactions with MHC class I and functional activities, there are some notable differences between the studies. Our studies in M553 cells suggest that the deletion of the transmembrane/cytosolic domains of tapasin had a more significant impact on the efficiency of tapasin–MHC class I binding than did ERp57 conjugation to tapasin (Figures 2 and 4). Immunoprecipitations with the anti-tapasin antibody by the Cresswell laboratory suggested a more critical role for tapasin–ERp57 binding in HLA-B*4402 recruitment to tapasin, following analyses of various tapasin mutants in 721.220/HLA-B*4402 cells (24). In addition, despite the lower efficiency of soluble tapasin–class I complex formation, we were able to detect complexes between soluble tapasin(C95A) and MHC class I heavy chains (Figures 2 and 4), whereas these complexes were not detectable in the other study (24). The observed differences may relate to the use of IFN-γ in our assays, which upregulates TAP as well as MHC class I subunits, promoting several of the interactions that are dependent on one or both of these proteins. TAP expression levels are very relevant to interactions mediated by full-length tapasin, and thus analyses under conditions where TAP expression is not limiting are important. It is alternatively possible that there are allele-specific or other cell type-specific differences in requirements of ERp57 associations versus the tapasin transmembrane/cytoplasmic domains for efficient tapasin–MHC class I binding. Our analyses examined tapasin binding to endogenously expressed MHC class I allotypes of M553 cells, which include HLA-A28, HLA-B*5701 and HLA-B*5001 (16). The Cresswell laboratory study examined interactions of exogenously expressed HLA-B*4402 in 721.220 cells which lack endogenous HLA-A and HLA-B, but express an endogenous HLA-C. It is possible that binding of tapasin to HLA-B*4402, a highly tapasin-dependent allotype (25), has more stringent requirements for accessory ER chaperones.

Our data indicate that tapasin promotes MHC class I assembly by two major mechanisms, involving (i) an ERp57-independent mode of tapasin function that requires the transmembrane and cytosolic domains of tapasin and involves associations with TAP (Figure 10A) and (ii) an ERp57-dependent mode of tapasin function requiring the ER luminal domains of tapasin and associations with calreticulin (Figure 10B). The ERp57-independent mode of tapasin function may involve the editing functions of tapasin which optimizes its peptide repertoire, as suggested using Fos-Jun tethered tapasin–MHC class I complexes (11). Furthermore, localization of MHC class I in the vicinity of the peptide source, TAP, could account for the ERp57-independent activity of tapasin. In some species such as chicken, which lack the counterpart of C95, the ERp57-independent mode of tapasin function may be the sole mechanism of tapasin function (26). Importantly, although the ERp57-independent mode of function requires the transmembrane and cytosolic domains of tapasin (Figure 1), the role of these domains

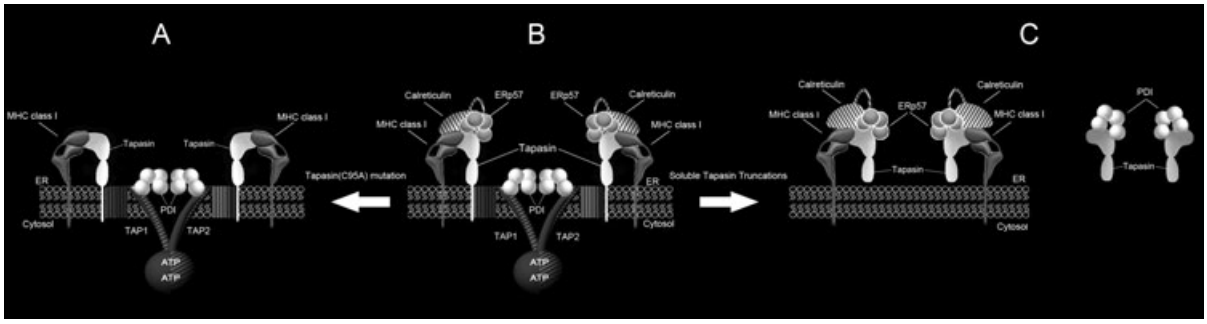

Figure 10: Two modes of tapasin function. A) (left) ERp57-independent mode of tapasin function. Studies with the tapasin(C95A) mutant indicate that tapasin is able to bind MHC class I molecules, and promote assembly of MHC class I molecules, directly and/or via localization of MHC class I in the vicinity of the TAP transporter. In IFN-γ-treated cells, the C95A mutation reduced the efficiency of tapasin–MHC class I binding compared with wild-type tapasin, but to a smaller extent than that induced by the soluble tapasin truncation. B) (middle): Combining both modes of tapasin function (A and C) contributes to strong binding interactions and function in the context of wild-type tapasin. PDI associates with TAP in a tapasin-independent manner, and may function as an initial acceptor for TAP-translocated peptides and/or promote degradation of unassembled TAP complex components. C) (right): ERp57-dependent mode of tapasin function. ERp57 binding to tapasin via C95 promotes assembly of MHC class I molecules directly and/or via the stabilization of calreticulin–MHC class I interaction. This activity of tapasin is observed with a soluble form of tapasin that is unable to associate with TAP, even though removal of the transmembrane and cytosolic domains of tapasin markedly destabilizes tapasin–MHC class I binding. Removal of the transmembrane and cytosolic domains of tapasin also induces C95-dependent conjugation of soluble tapasin with PDI.

extends beyond the previously suggested functions for these domains in TAP stabilization (4) (Figures 2, 4 and 5).

Tapasin-dependent recruitment of ERp57 enhanced the ability of human tapasin to mediate MHC class I assembly (Figure 1), even under conditions where tapasin–MHC class I interactions were relatively weak (soluble tapasin; Figures 2 and 4). ERp57 and calreticulin interact outside of the MHC class I assembly complex (19), and higher representation of ERp57 in conjugation with purified tapasin correlated with increased calreticulin binding *in vitro* (Figure 9F). Tapasin-C95-mediated recruitment of ERp57 and enhanced recruitment of calreticulin contributed to enhanced calreticulin–MHC class I binding and increased stabilities of MHC class I heavy chains (Figures 1A,B, 2 and 4). Thus, calreticulin is likely an important player in the ERp57-dependent functional activity of tapasin, but further studies are needed to understand how calreticulin interacts with MHC class I and tapasin, and the extent of its contribution to the functional activity of tapasin. It is widely believed that binding monoglucosylated glycans is sufficient to recruit calreticulin to substrates. However, the findings reported here indicate that multiple tapasin-dependent interactions rather than glycan binding alone contribute to efficient recruitment of calreticulin to the MHC class I assembly complex. Further understanding of the mechanisms of calreticulin recruitment into the MHC class I assembly complex will allow insights into whether similar mechanisms could be used to promote the recruitment of ER chaperones to enhance the assembly of other multiprotein complexes, particularly of viruses.

The recent crystal structure analysis of a soluble tapasin–ERp57 heterodimer showed that both catalytic domains of ERp57 (a and a′ domain) are involved in tapasin binding (7). ERp57 residues involved in binding to tapasin are conserved in PDI (7). Specificity of tapasin–ERp57 heterodimer formation was attributed to differences in inter-domain orientations between different PDI family members. A shorter distance was noted between Cα atoms of C57 and C406 of ERp57 in the tapasin–ERp57 heterodimer (7), compared with counterpart PDI residues in the yeast PDI structure which was crystallized as free protein rather than in a substrate-conjugated form (27). Our studies indicate that soluble tapasin *per se* is not fully specific for ERp57 conjugation as conjugates between soluble tapasin and PDI were also readily detectable, although at a level approximately 7.5-fold lower than that of ERp57 (Figures 7 and 8 and Figure S1).

How might TAP binding inhibit tapasin–PDI binding and promote tapasin–ERp57 interaction specificity? Cooperative interactions that stabilize the heptameric complexes involving TAP1/TAP2/tapasin/MHC class I/calreticulin/ERp57 via multimodal binding between the different components must impose a strong structural constraint on the complete complex, which is absent in the corresponding soluble tapasin complexes. The lack of complex stability in soluble tapasin complexes is likely directly responsible for the reduction in oxidoreductase conjugation specificity. Thus, structural constraints of the complete MHC class I assembly complex contribute to the specificity of tapasin–ERp57 binding.

We show that PDI is likely a *bona fide* component of the TAP complex not by its ability to conjugate with tapasin but rather by its ability to bind to TAP (Figure 6). TAP-associated PDI has been implicated in the maintenance of oxidized forms of MHC class I heavy chains, as higher levels of reduced heavy chains were found in PDI-depleted cells (13). However, the majority of TAP-associated heavy chains were oxidized in PDI-depleted cells (13), which suggests that PDI did not have a major influence on maintaining oxidized forms of TAP-associated heavy chains. The possibility of a function for TAP-associated PDI in mediating tapasin oxidation is suggested by the findings that TAP-associated forms of tapasin are more oxidized compared with Pasta-1-associated forms of tapasin (data not shown); however, the oxidized form of tapasin found in complex with TAP may also simply result from steric constraints of reductase access to TAP-associated forms of tapasin, rather than PDI-dependent catalytic oxidation. The relevant role of TAP-associated PDI may relate to the sequestration of TAP-translocated peptides, to prevent their premature retro-translocation, as previously suggested (13,28). Alternatively, since the presence of functional forms of TAP-associated tapasin reduced the extent of PDI–TAP binding (Figures 6A,C), it is also possible that PDI functions in the retro-translocation and degradation of components of the TAP complex, including TAP itself, when not stabilized by a complete repertoire of associated factors. PDI binding to TAP may involve interactions with surface hydrophobic patches on PDI (27). Further functional studies will be needed to assess whether TAP-associated PDI represents a specific mechanism for mediating peptide retention in the ER, or peptide loading complex (PLC) component degradation. It is a formal possibility that the observed TAP–PDI complex represents a more non-specific hydrophobic interactions-based binding.

Our studies also allowed a direct assessment of the effects of ERp57 and TAP binding on tapasin folding. Abrogation of C95-mediated conjugate formation did not induce significant soluble tapasin(C95A) aggregation in cell lysates, and soluble tapasin(C95A) migrated predominantly as monomers (data not shown). However, soluble wild-type tapasin was aggregated when purified from cell supernatants, even when co-expressed with ERp57 (Figure 9A,D), suggesting that in addition to oxidoreductase binding, interactions with ER lumenal factors such as calreticulin and GRP78 may be important for maintaining tapasin stability and inhibiting its aggregation (Figure 9B).

In summary, we show that tapasin functions by two major mechanisms, involving (i) binding of MHC class I molecules via interactions involving its ER lumenal *and*

transmembrane/cytosolic domains and (ii) recruitment of ERp57 and calreticulin into the MHC class I assembly complex (Figure 10). Further studies are required to understand whether the tapasin transmembrane and cytosolic domains directly impact tapasin–MHC class I binding, or whether TAP/tapasin binding impacts the efficiency of tapasin–MHC class I binding. Alternatively, the transmembrane domain of tapasin could induce binding merely by increasing the local concentrations of tapasin in membranes containing MHC class I. In addition, whether the ERp57-independent functional activity of tapasin results in part from its ability to promote physical interactions between MHC class I and TAP (thus achieving a higher local concentration of peptides) also remains to be investigated. Furthermore, modes of calreticulin interaction and function remain to be defined, as also the precise function of TAP-associated PDI.

Materials and Methods

Cell lines

M553 cells (obtained from Dr Naveen Bangia (16) and HeLa cells were grown in RPMI 1640 and DMEM (Invitrogen), respectively, supplemented with 10% FBS and penicillin–streptomycin. Chinese hamster ovary (CHO) cells expressing tapasin or tapasin and ERp57 were grown in alpha-MEM media (Invitrogen) supplemented with 5% dialyzed FBS and antibiotics–antimycotics (Invitrogen).

Retroviral constructs

The construction of retroviral vectors encoding tapasin and influenza hemagglutinin (HA)-tagged HLA-A2 has been previously described (22,29). The C95A mutant of full-length tapasin was generated using the QuikChange site-directed mutagenesis kit and full-length tapasin in the pAcUW51 vector using the following oligonucleotides, 5-ACCCCC GCGCAGAACGCCCCGCGGGCCCTGGAT-3 and 5-ATCCAGGGCCCGCGG GGCGTTCTGCGCGGGGGT-3. Mutant clones were sequenced and ligated into pMSCV-puro. The C95A mutant of soluble FLAG-tagged tapasin was generated by site-directed mutagenesis of soluble tapasin in the pBJ5-GS vector (10) using the oligonucleotides described above. Mutant or wild-type soluble tapasin were sequenced and ligated into pMSCV-puro. Viruses were generated as previously described (30,31) using BOSC cells, and used to infect M553 cells. Retrovirus infectivity to human cells was achieved by pseudotyping the retroviral envelope with the vesicular stomatitis virus G protein. M553 cells were transduced with retroviruses encoding HA-HLA-A2, and selected by treatment with 1 mg/mL Geneticin (Invitrogen), and maintained in 0.5 mg/mL Geneticin (this cell line is designated as M553/A2). After verifying M553/A2 expression by flow cytometric analyses and by immunoblotting analyses of cell lysates, M553 or M553/A2 cells were transduced with the different tapasin-encoding retroviruses, and selected by treatment with 1 μg/mL puromycin (Sigma). Cells were maintained in 0.5 μg/mL puromycin.

Fluorescence-activated cell sorting analysis to assess MHC class I cell surface expression

A total of 2×10^6 cells were washed 3× with fluorescence-activated cell sorter (FACS) buffer (PBS pH 7.4 containing 1% FBS). Cells were then incubated with anti-HA ascites (Covance Scientific) or W6/32 ascites fluid (a human MHC class I heterodimer-specific antibody) (32) at a 1:250 dilution for 1 h on ice. Following this incubation, cells were washed 3× with FACS buffer. Cells were then incubated for 1 h on ice with fluorescein isothiocyanate (FITC)-conjugated goat anti-mouse immunoglobulin G (IgG) (Jackson Laboratories) at 1:250 dilutions, followed by three washes with FACS buffer. Cells were then analyzed using a FACS-Canto cytometer and WINMDI software (Joe Trotter, The Scripps Institute, Flow Cytometry Core Facility).

Immunoprecipitation and immunoblotting analysis

Three-six confluent 100×20 mm plates (4×10^6 cells per plate) of M553/A2 or M553 cells expressing different tapasin constructs were treated with 500 IU IFN-γ (PeproTech) for 48 h and processed for different immunoprecipitation as described below. IFN-γ treatment of cells was used to up-regulate TAP and promote TAP-mediated binding interactions.

To study tapasin and MHC class I binding to various proteins (Figures 2 and 4), the IFN-γ-treated M553/A2 or M553 cells were harvested and washed in PBS pH 7.4. The cells were then incubated with membrane-permeable cross-linker (4 mM DTBP) in PBS pH 8.2 for 1 h at room temperature followed by incubation with 1 M Tris pH 7.4 for 15 min at room temperature to quench free cross-linker. The cells were then washed once with PBS pH 7.4 and lysed in lysis buffer (25 mM Tris, 150 mM NaCl, 0.2 mM $CaCl_2$, 1% digitonin and protease inhibitors) for 1 h on ice. The lysates were centrifuged at 4°C for 30 min and protein concentration in lysates was determined by a bicinchoninic acid (BCA) protein assay (Pierce, Thermo Scientific). Equal microgram amounts of lysates were incubated with anti-tapasin (Pasta-1; (6) obtained from Dr. Peter Cresswell) or HC10 (33) overnight at 4°C. Following overnight incubation, immunoprecipitates were isolated with protein G beads for 2 h at 4°C. The beads were washed three times with lysis buffer containing 0.1% digitonin, resuspended in reducing or non-reducing SDS-PAGE buffer and boiled. The proteins were separated by SDS-PAGE and analyzed by western blotting using the enhanced chemiluminescence (ECL) Plus Kit (Amersham, GE Healthcare). Immunoblotting analyses of the Pasta-1 and HC10-based immunoprecipitations were undertaken with the following antibodies; rabbit anti-tapasin antisera (antisera generated against an N-terminal peptide of tapasin) obtained from Dr Ted Hanson (Washington University) the HC10 antibody (33) for MHC class I heavy chains, rabbit polyclonal anti-ERp57 antibody (Santa Cruz Biotechnology, Inc.) and rabbit polyclonal anti-calreticulin (Stressgen). The secondary antibodies used were Peroxidase AffiniPure goat anti-rabbit IgG (heavy and light chain) or Peroxidase AffiniPure goat anti-mouse IgG (heavy and light chain) (Jackson ImmunoResearch Laboratories, Inc.).

TAP binding was analyzed both in the absence (M553 cells) and in the presence (M553/A2 cells) of cross-linking agent. For these analyzes, IFN-γ-treated M553 cells expressing different tapasin constructs were harvested and washed in PBS pH 7.4. The cells were then lysed in lysis buffer (25 mM Tris, 150 mM NaCl, 0.2 mM $CaCl_2$, 1% digitonin and protease inhibitors) for 1 h on ice. M553/A2 cells were first incubated with 4 mM DTBP in PBS pH 8.2 for 1 h at room temperature. The cells were then washed once with PBS pH 7.4 after quenching the free cross-linker and lysed as described for the M553 cells. Lysates were immunoprecipitated with anti-TAP1 antisera (34) obtained from Dr M. J. Androlewicz (Lee Moffit Cancer Center) and processed as above. HeLa cells were also processed for TAP1 immunoprecipitation as above. For anti-TAP1 immunoprecipitations, the following antibodies were used: mouse anti-TAP1 (SB05 212) or mouse anti-tapasin (35) obtained from Dr Soldano Ferrone, HC10 (33) to detect MHC class I heavy chains, mouse anti-PDI monoclonal antibody (Abcam), mouse anti-ERp57 monoclonal antibody (Abcam), goat polyclonal anti-calreticulin (Santa Cruz). The secondary antibodies used were Peroxidase AffiniPure goat anti-mouse IgG (heavy and light chain) or Peroxidase AffiniPure bovine anti-goat IgG (heavy and light chain) (Jackson ImmunoResearch Laboratories, Inc.).

Metabolic labeling and endo-glycosidase H sensitivity

To study the rates of intracellular trafficking of MHC class I in M553 or M553 cells expressing full-length tapasin(C95A), cells were pulsed with

0.1 mCi [S^{35}]methionine-cysteine and chased for 0, 30, 60 and 120 min. The cells were then lysed in 1% digitonin, precleared for 2 h with protein G beads and lysates were immunoprecipitated with W6/32 antibody. The IPs were processed as described for other IPs and divided into two equal aliquots. One set of aliquots were treated with Endo-H for 1 h at 37°C. Following Endo-H digestion, the samples were resolved by SDS–PAGE and developed by phosphorimaging analysis.

Tapasin-oxidoreductase conjugate formations (Figure 7)

For these analyses, IFN-γ-treated cells were harvested and incubated with 2 mM MMTS (Pierce) in PBS pH 7.4 for 10 min on ice. MMTS was used alone without DTBP. The cells were then pelleted and lysed in lysis buffer containing 1% digitonin and 10 mM MMTS. Equal microgram amounts of lysates were incubated with anti-tapasin (Pasta-1; (6) obtained from Dr Peter Cresswell) overnight at 4°C. Samples were processed for immunoblotting analyses as described above.

Protein purifications (Figures 8 and 9)

Twelve confluent 100 × 20 mm plates of M553 cells expressing soluble tapasin were harvested and washed with PBS pH 7.4. The cells were lysed in lysis buffer (50 mM sodium phosphate, pH 7.0, 10 mM MMTS, 1% Triton-X-100 and protease inhibitors) for 1 h on ice. MMTS was used alone and not used in combination with DTBP. For CHO cell experiments, 20 confluent plates of CHO cells (100 × 20 mm) expressing tapasin or tapasin and ERp57 were harvested and washed with PBS pH 7.4. The cells were lysed as above. The lysates were centrifuged at 4°C for 30 min and loaded onto an anti-FLAG agarose column (Sigma). The column was washed with 50 mM sodium phosphate buffer containing 1% Triton-X-100 and 2 mM MMTS, then with 50 mM sodium phosphate buffer alone, and proteins eluted using FLAG peptide. Proteins were concentrated and separated by gel filtration chromatography. Different fractions were analyzed for the presence of tapasin, ERp57 and PDI by immunoblotting analyses. To determine the relative amounts of PDI and ERp57 that were associated with soluble tapasin following gel filtration analysis, two different methods were used. The soluble tapasin conjugates or different amounts of purified ERp57 and PDI proteins (ProSpec) were separated by SDS–PAGE and immunoblotting analyses undertaken with anti-PDI (Santa Cruz Biotechnology, Inc.) and anti-ERp57 (Santa Cruz Biotechnology, Inc).The blots were scanned and relative band intensities were quantified using IMAGEQUANT software. Signals for purified ERp57 and PDI were plotted as a function of protein concentration, and analyzed by Prism to estimate the amounts of ERp57 and PDI present in the conjugate fractions. In a second analysis, the complexes were resolved by SDS–PAGE, Coomassie Blue stained, and indicated bands excised and submitted for mass spectrometric analyses. Relative amounts of each protein were estimated by comparing average intensities of 10 most abundant peptides for each protein (Figure S1).

For proteins purified from CHO cells, eluted proteins were separated by SDS–PAGE, Coomassie Blue stained and indicated bands were subjected to mass spectrometric analysis. All mass spectrometric analyses were conducted at the Taplin Biological Mass Spectrometry Facility (Harvard Medical School). Protein purifications from CHO cells supernatants were undertaken as previously described (10).

Full-length human calreticulin (hCRT) lacking the signal sequence was generated using ligation-independent cloning (LIC). The sequence was amplified by polymerase chain reaction (PCR) using primers that allowed for subsequent LIC into the pMCSG7 vector. The following oligonucleotide primers were used; Forward: 5′ TACTTCCAATCCAATGCTGTCGCCGAGCCTGC 3′ and Reverse: 5′ TTATCCACTTCCAATGTTACAGCTCGTCCTTGGC 3′ The purified constructs contain an N-terminal MHHHHHHSSGVDLGT*ENLYFQ*SNA fusion sequence. The protein was induced at room temperature overnight and purified using nickel beads according to the standard protocol. The protein was further purified by gel filtration column and stored at −20°C in 10% glycerol.

Expression of tapasin and ERp57 in CHO cells

ERp57 lacking the ER retention sequence was amplified using the following oligonucleotides: 5-AAGCGGCCGCCAGCTGCCACCATGCGCCTCCGCCGC-3 and 5-ATGCGGCCGCGGTACCTTATGCCTTCTTCTTCTT-3 and cloned into the pBJ5GS vector using *Bam*HI and *Not*1 sites. CHO cells were transfected with pBJ5-GS vector expressing tapasin and ERp57 by the lipofectin protocol and cells were selected with methionine sulfoximine as previously described (10). Clones surviving selection were screened for expression of tapasin and ERp57 by immunoprecipitations of cell supernatants with anti-FLAG (Sigma) and anti-ERp57 monoclonal antibody (Abcam) antibodies, following metabolic labeling of cells (10). Cells expressing both proteins were clonally amplified, and clones re-tested for expression of both proteins by metabolic labeling and co-immunoprecipitation analyses, prior to large-scale amplification and protein purifications as described above.

ELISA procedures

For these assays, tapasin was purified from lysates of CHO cells under three different conditions (i) CHO–tapasin cells lysed in the absence of MMTS (ii) CHO–tapasin cells lysed in the presence of MMTS or (iii) CHO–tapasin–ERp57 cells lysed in the presence of MMTS. An anti-FLAG column was used for purifying protein under each condition, as described above. The protein concentrations were estimated by a BCA assay. The ELISA plates (BD Falcon) were coated by overnight incubation at 4°C with 1–2 μg of each type of tapasin, or BSA in PBS pH 7.4. Unbound proteins were removed by washing the wells 3× with ELISA buffer (50 mM Tris, 150 mM NaCl, 0.5 mM $CaCl_2$) containing 0.5% Tween-20 (Sigma). The wells were blocked with 10% FBS in ELISA buffer at 37°C for 1 h and excess FBS was removed. To study calreticulin binding to tapasin, 1–2 μg of human calreticulin in ELISA buffer was added and plates were incubated at 37°C for 3 h. Unbound calreticulin was removed, anti-calreticulin antibody (goat anti-calreticulin) was added and plates incubated at 37° C for 1 h. The primary antibody was washed, secondary antibody (bovine anti-goat horseradish peroxidase) added, prior to further incubation at 37°C for 1 h. After washing the wells three times with ELISA buffer containing 0.5% Tween-20, developer solution (BD Falcon) was added. The developer reaction was stopped by adding 2 N H_2SO_4 and absorbance read at 450 nm.

Acknowledgments

We thank Christopher Perria for early contributions to the project. We sincerely thank our colleagues, Dr. Naveen Bangia for the M553 cell line, Dr. Kathleen Collins for the retroviral construct encoding HA-tagged HLA-A2, Drs Matt Androlewicz, Peter Cresswell, Soldano Ferrone and Ted Hansen for the antibody reagents. We thank the University of Michigan DNA sequencing core for sequencing analyses, and the hybridoma core for antibody production. This work was supported by a National Institutes of Health grant AI-044115 (to M. R.) and by financial support from the Michigan Diabetes Research and Training Center and the Rheumatic Diseases Core Center of the University of Michigan.

Supporting Information

Additional Supporting Information may be found in the online version of this article:

Figure S1: Association of ERp57 and PDI with soluble tapasin in M553 cells. A total of 4.8×10^7 M553/soluble tapasin cells were lysed in the presence of MMTS (no cross-linker) and immunoprecipitated with anti-FLAG beads. The anti-FLAG eluates were run on a gel filtration column to isolate soluble tapasin and associated proteins. Gel filtration fractions containing ERp57/PDI and soluble tapasin were concentrated, protein separated by SDS–PAGE and Coomassie Blue staining, and indicated

bands (Figure 8B) were subjected to mass spectroscopic analysis. The most abundant proteins identified in band 2 (Figure 8B) were ERp57 and PDI. The bar graphs show 10 of the most abundant peptides identified for ERp57 (A) and PDI (B). The NL (relative peptide abundance) values of top 10 peptides were used to estimate the relative amounts of each protein associated with soluble tapasin.

Please note: Wiley-Blackwell are not responsible for the content or functionality of any supporting materials supplied by the authors. Any queries (other than missing material) should be directed to the corresponding author for the article.

References

1. Raghavan M, Del Cid N, Rizvi SM, Peters LR. MHC class I assembly: out and about. Trends Immunol 2008;29:436–443.
2. Li S, Sjogren HO, Hellman U, Pettersson RF, Wang P. Cloning and functional characterization of a subunit of the transporter associated with antigen processing. Proc Natl Acad Sci U S A 1997;94:8708–8713.
3. Ortmann B, Copeman J, Lehner PJ, Sadasivan B, Herberg JA, Grandea AG, Riddell SR, Tampe R, Spies T, Trowsdale J, Cresswell P. A critical role for tapasin in the assembly and function of multimeric MHC class I-TAP complexes. Science 1997;277:1306–1309.
4. Lehner PJ, Surman MJ, Cresswell P. Soluble tapasin restores MHC class I expression and function in the tapasin-negative cell line 220. Immunity 1998;8:221–231.
5. Garbi N, Tiwari N, Momburg F, Hammerling GJ. A major role for tapasin as a stabilizer of the TAP peptide transporter and consequences for MHC class I expression. Eur J Immunol 2003; 33:264–273.
6. Dick TP, Bangia N, Peaper DR, Cresswell P. Disulfide bond isomerization and the assembly of MHC class I-peptide complexes. Immunity 2002;16:87–98.
7. Dong G, Wearsch PA, Peaper DR, Cresswell P, Reinisch KM. Insights into MHC class I peptide loading from the structure of the tapasin–ERp57 thiol oxidoreductase heterodimer. Immunity 2009;30: 21–32.
8. Wearsch PA, Cresswell P. Selective loading of high-affinity peptides onto major histocompatibility complex class I molecules by the tapasin-ERp57 heterodimer. Nat Immunol 2007;8:873–881.
9. Peaper DR, Cresswell P. The redox activity of ERp57 is not essential for its functions in MHC class I peptide loading. Proc Natl Acad Sci U S A 2008;105:10477–10482.
10. Rizvi SM, Raghavan M. Direct peptide regulatable interactions between tapasin and MHC class I molecules. Proc Natl Acad Sci 2006;103:18220–18225.
11. Chen M, Bouvier M. Analysis of interactions in a tapasin/class I complex provides a mechanism for peptide selection. EMBO J 2007;26:1681–1690.
12. Simone LC, Wang X, Tuli A, McIlhaney MM, Solheim JC. Influence of the tapasin C terminus on the assembly of MHC class I allotypes. Immunogenetics 2009;61:43–54.
13. Park B, Lee S, Kim E, Cho K, Riddell SR, Cho S, Ahn K. Redox regulation facilitates optimal peptide selection by MHC class I during antigen processing. Cell 2006;127:369–382.
14. Wearsch PA, Cresswell P. The quality control of MHC class I peptide loading. Curr Opin Cell Biol 2008;20:624–631.
15. Peaper DR, Wearsch PA, Cresswell P. Tapasin and ERp57 form a stable disulfide-linked dimer within the MHC class I peptide-loading complex. EMBO J 2005;24:3613–3623.
16. Belicha-Villanueva A, McEvoy S, Cycon K, Ferrone S, Gollnick SO, Bangia N. Differential contribution of TAP and tapasin to HLA class I antigen expression. Immunology 2008;124:112–120.
17. Tan P, Kropshofer H, Mandelboim O, Bulbuc N, Hammerling GJ, Momburg F. Recruitment of MHC class I molecules by tapasin into the transporter associated with antigen processing-associated complex is essential for optimal peptide loading. J Immunol 2002;168:1950–1960.
18. Procko E, Raghuraman G, Wiley DC, Raghavan M, Gaudet R. Identification of domain boundaries within the N-termini of TAP1 and TAP2 and their importance in tapasin binding and tapasin-mediated increase in peptide loading of MHC class I. Immunol Cell Biol 2005;83:475–482.
19. Frickel EM, Riek R, Jelesarov I, Helenius A, Wuthrich K, Ellgaard L. TROSY-NMR reveals interaction between ERp57 and the tip of the calreticulin P-domain. Proc Natl Acad Sci U S A 2002;99:1954–1959.
20. Grandea AG, 3rd, Golovina TN, Hamilton SE, Sriram V, Spies T, Brutkiewicz RR, Harty JT, Eisenlohr LC, Van Kaer L. Impaired assembly yet normal trafficking of MHC class I molecules in Tapasin mutant mice. Immunity 2000;13:213–222.
21. Garbi N, Tanaka S, Momburg F, Hammerling GJ. Impaired assembly of the major histocompatibility complex class I peptide-loading complex in mice deficient in the oxidoreductase ERp57. Nat Immunol 2006;7:93–102.
22. Thammavongsa V, Raghuraman G, Filzen TM, Collins KL, Raghavan M. HLA-B44 polymorphisms at position 116 of the heavy chain influence TAP complex binding via an effect on peptide occupancy. J Immunol 2006;177:3150–3161.
23. Molinari M, Helenius A. Glycoproteins form mixed disulphides with oxidoreductases during folding in living cells. Nature 1999;402:90–93.
24. Vigneron N, Peaper DR, Leonhardt RM, Cresswell P. Functional significance of tapasin membrane association and disulfide linkage to ERp57 in MHC class I presentation. Eur J Immunol 2009;39:2371–2376.
25. Williams AP, Peh CA, Purcell AW, McCluskey J, Elliott T. Optimization of the MHC class I peptide cargo is dependent on tapasin. Immunity 2002;16:509–520.
26. Frangoulis B, Park I, Guillemot F, Severac V, Auffray C, Zoorob R. Identification of the Tapasin gene in the chicken major histocompatibility complex. Immunogenetics 1999;49:328–337.
27. Tian G, Xiang S, Noiva R, Lennarz WJ, Schindelin H. The crystal structure of yeast protein disulfide isomerase suggests cooperativity between its active sites. Cell 2006;124:61–73.
28. Spee P, Neefjes J. TAP-translocated peptides specifically bind proteins in the endoplasmic reticulum, including gp96, protein disulfide isomerase and calreticulin. Eur J Immunol 1997;27:2441–2449.
29. Roeth JF, Williams M, Kasper MR, Filzen TM, Collins KL. HIV-1 Nef disrupts MHC-I trafficking by recruiting AP-1 to the MHC-I cytoplasmic tail. J Cell Biol 2004;167:903–913.
30. Pear WS, Nolan GP, Scott ML, Baltimore D. Production of high-titer helper-free retroviruses by transient transfection. Proc Natl Acad Sci U S A 1993;90:8392–8396.
31. Van Parijs L, Refaeli Y, Lord JD, Nelson BH, Abbas AK, Baltimore D. Uncoupling IL-2 signals that regulate T cell proliferation, survival, and Fas-mediated activation-induced cell death. Immunity 1999;11:281–288.
32. Parham P, Barnstable CJ, Bodmer WF. Use of a monoclonal antibody (W6/32) in structural studies of HLA-A,B,C, antigens. J Immunol 1979;123:342–349.
33. Stam NJ, Vroom TM, Peters PJ, Pastoors EB, Ploegh HL. HLA-A- and HLA-B-specific monoclonal antibodies reactive with free heavy chains in western blots, in formalin-fixed, paraffin-embedded tissue sections and in cryo-immuno-electron microscopy. Int Immunol 1990;2:113–125.
34. Androlewicz MJ, Ortmann B, van Endert PM, Spies T, Cresswell P. Characteristics of peptide and major histocompatibility complex class I/beta 2-microglobulin binding to the transporters associated with antigen processing (TAP1 and TAP2). Proc Natl Acad Sci U S A 1994;91:12716–12720.
35. Ogino T, Wang X, Kato S, Miyokawa N, Harabuchi Y, Ferrone S. Endoplasmic reticulum chaperone-specific monoclonal antibodies for flow cytometry and immunohistochemical staining. Tissue Antigens 2003;62:385–393.